Integrated Ground Reaction Force Sensing and Terrain Classification for Small Legged Robots

X. Alice Wu[1], Tae Myung Huh[1], Rudranarayan Mukherjee[2], and Mark Cutkosky[1]

***Abstract*—We present the design and implementation of a miniature tactile sensing array for ground reaction force measurements in small legged robots. Dynamic ground pressure data from the sensors were collected using a small two-legged runner and used to train a support vector machine (SVM) terrain classifier. Results show that tactile sensing data, in combination with information about the motor torque and robot gait, are sufficient to distinguish among hard, slippery, grassy and granular terrain types with >90% accuracy in a single stride. The most useful classifier features include stride frequency, peak motor torque, and peak and average tactile sensor readings.**

***Index Terms*—Force and Tactile Sensing, Multilegged Robots**

I. Introduction

FOR small legged robots and animals, the details of interactions between their feet and the ground can have a profound effect on the speed and efficiency of locomotion. For example, on grassy or granular terrain, the interactions may dissipate significant energy due to friction as the feet deform the surface. Conversely on hard and smooth surfaces, slippage may be significant. Perhaps of most interest are leg and ground interactions on granular media such as sand and loose soil, which can have a considerable effect on limb kinematics and locomotion performance [1,2].

Small animals use numerous mechanorceptors in their legs and feet to monitor foot/ground interactions and adjust their gait and speed accordingly. For example, in insects, campaniform sensilla and sensory hairs provide a dynamic measure of contacts and loads in the limbs [3]. However, until very recently, practical considerations including sensor size, robustness and wiring have made it difficult to equip small robots with anything approaching the sensory capabilities of small legged animals. Dynamic tactile sensing on the feet would allow small robots to sense the magnitude and location of ground contact. Sensor information would also allow robots to identify the terrain type and perform gait adjustments for more efficient locomotion.

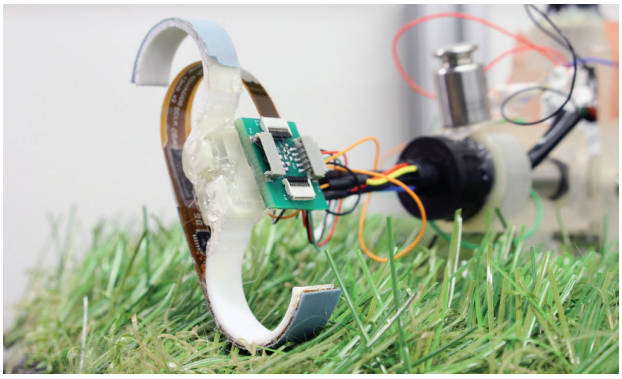

Fig. 1: An instrumented curved leg on a two-legged runner in grassy terrain.

The main contribution of this paper is the use of an array of miniature capacitive tactile sensors to directly measure ground reaction forces (GRF) on the legs of small running robots. The sensors are implemented on a curved C-shape leg as this form factor is common in small legged robots [1,4,5]; however the flexible design can be adapted to suit a wide variety of appendage shapes and sizes. We first demonstrate the tactile sensor's ability to measure spatially-distributed normal GRF over a variety of surfaces. We then show that dynamic GRF sensing data allow us to segment running data into individual strides and train a machine learning classifier to perform terrain identification based on the magnitude and distribution of forces on the legs in combination with motor torque and stride frequency. Results are presented, with insights into sensor features important to accurate terrain classification.

II. Related Work

A. Ground Reaction Sensing

Numerous efforts have been made to perform terrain identification in larger mobile vehicles. Examples include the use of dynamic vibration signals from inertial measurement units (IMUs) and current/voltage measurements from motors attached to the wheels or legs [6]–[10]. Others utilize vision systems [11]–[15], sound [16], or tactile probes attached to a robot traversing through various terrains [17]. Other investigators measure ground reaction forces directly using force torque sensors [18,19] or tactile sensing arrays [20,21] mounted on the feet.

In addition to terrain classification, ground reaction forces can be used for feedback-control in larger mobile vehicles,

Manuscript received: August 31, 2015; Revised December 17, 2015; Accepted January 13, 2016.

This paper was recommended for publication by Editor John Wen upon evaluation of the Associate Editor and Reviewers' comments. This work is supported in part by the Army Research Laboratory under the Micro Autonomous Systems and Technology Collaborative Technology Alliance. Alice Wu is supported by the NSF Graduate Research Fellowship. Tae Myung Huh is supported by the Samsung Scholarship.

[1]X. Alice Wu, Tae Myung Huh, and Mark Cutkosky are with The Center for Design Research, Stanford University, Stanford, CA 94305, USA axwu@stanford.edu; taemyung@stanford.edu; cutkosky@stanford.edu

[2]Rudranarayan Mukherjee is with NASA Jet Propulsion Laboratory, California Institute of Technology, Pasadena, CA 91101, USA rudranarayan.m.mukherjee@jpl.nasa.gov

Digital Object Identifier (DOI): see top of this page.

where the time constant permits within-stride response. Investigations have included the use of ground reaction forces to analyze stability via load transfer metrics [22,23] and to optimize traction via constraints on friction [24]–[26].

Recent efforts have also been directed toward instrumenting small legged robots with binary hair arrays, body tactile bumpers, and leg strain sensing [27]. Others have employed a large tactile array as an instrumented ground surface [28] and performed terrain classification on small robots using statistical moments of data sampled from on-board IMUs and joint currents [29].

B. Tactile Sensing Technology

As detailed in several sensor review papers [30]–[33], many transduction methods have been employed to measure contact forces and pressure distributions including optical [34]–[37], resistive [38]–[41], magnetic [42,43], and capacitive [44]–[47]. Among these, optical and magnetic sensors that measure deflections in a relatively thick, compliant skin are unsuitable for the present application because they add too much bulk and weight. In addition, some approaches, such as those based on optical fibers, are challenging to adapt to legs that undergo continuous rotation. Among other transduction technologies, piezoresistive sensors based on conductive inks or polymers are inexpensive and robust, but typically suffer from substantial hysteresis, which limits their use for dynamic tactile sensing [30]. Another possibility is to pattern strain gages directly onto the feet, but this solution requires instrumentation quality amplifiers and again presents challenges for wiring between continuously rotating legs and the robot body.

In comparison to other tactile sensing technologies, capacitive sensors have enjoyed a recent increase in popularity due to the availability of inexpensive surface-mounted capacitance to digital converters (CDCs) to provide active shielding, signal processing and digital communication. Examples include sensors for robot hands [48,49] and miniature surgical grippers [50]. In the present application, capacitive tactile sensors based on flexible circuits with surface-mounted CDCs are attractive due to their low weight, robustness, and ability to wrap around various geometries. For robots with rotary legs, the minimization of wiring is an additional advantage.

III. Sensor Design and Integration

A. Sensor and Leg Assembly

The sensors used here build upon a design introduced in [47]. In this design, a sparse structure of silicone rubber is used as the dielectric in a capacitive tactile sensor, which is easily modified to match the desired force range and sensitivity for a particular application.

The inner structure of the sensor assembly consists of a 4-layer, $156\,\mu\mathrm{m}$, $8\,\mathrm{mm}$ wide polyimide flex circuit (FPBC) with 5 force sensing pads ($25\,\mathrm{mm}^2$ each), as seen in Fig. 2. Blind vias minimize stray capacitance to both the external sensing pads and the internal active shielding layers, allowing us to achieve a high signal to noise ratio. The outer layer consists of a sheet of conductive fabric (Less EMF RadioScreen). The dielectric is an array of posts (TAP Silicone RTV, E = 840 kPa, fill ratio = 16%) and is cast in place on the underside of the fabric. To improve traction, another thin layer of silicone is cast onto the outer surface of the conductive fabric.

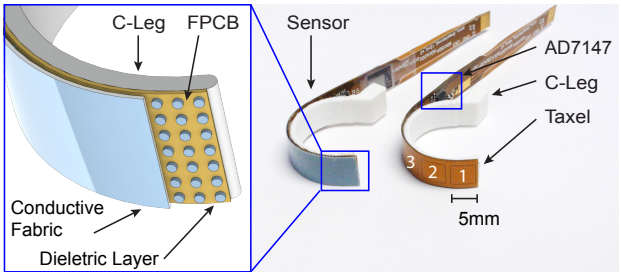

Fig. 2: Sensor/leg assembly. The sensor consists of 5 taxels, with taxel 1 at the tip of the leg (distal) and taxel 5 near the hip (proximal); sensor assembly cross-section shown on left.

To acquire ground reaction force data, the inner layer of the sensor is bonded to a 3D-printed (Stratasys ABSplus) curved robot leg (10mm wide, 30mm long measured from hip to toe) with an adhesive (Loctite 401). The outer layer is then bonded to the inner layer with a thin silicone adhesive (Smooth-On, Inc. Sil-Poxy). The total sensor assembly (excluding leg) weighs 0.95 g.

A 16-bit CDC (Analog Devices AD7147) samples the sensing pads at $\sim$260 Hz. Sensor data are acquired via I^2C through a microcontroller (Microchip PIC24F04KA201) and sent to a PC via USB through slip rings.

B. Performance Analysis

1) Calibration: The curved sensor/leg assembly was calibrated using an Aurora Scientific Inc. 309C Dual-Mode Muscle Lever System, which applied a $0.5\,\mathrm{Hz}$ sinusoidal input force between $0\,\mathrm{N}$ and $5\,\mathrm{N}$ for 10 successive cycles. A custom linear bearing setup constrained the leg's motion uniaxially, with the leg orientation adjusted to bring each taxel in contact with a force plate. Ground forces were measured using a commercial force/torque sensor (ATI Gamma SI-32-2.5, accuracy: $\pm 0.05\,\mathrm{N}$). Taxel pressure measurements over this range demonstrate low hysteresis and are slightly nonlinear, which can be accommodated using a polynomial fit [47]. Fig. 3 shows typical calibrated sensor data as compared to forces measured on the ATI load cell for uniaxial compressive loads; due to bending of the leg, the match is close but not exact at the peak forces.

2) Static and Dynamic Performance: The sensitivity of the sensor is $670\,\mathrm{counts/N}$ averaged across 5 taxels. The RMS noise is 9 counts at 260 Hz sampling rate, and thus limits the effective resolution to 12 bits. The minimum resolvable normal force is 13 mN or 1.3 grams. Although the sensor has previously been tested for loads up to 100N in compression, the maximum static force in this application is approximately $10\,\mathrm{N}$ without incurring structural damage to the leg. Dynamic response of an equivalent sensor was previously characterized in [51]. The experimental transfer function estimate (ETFE) of the sensor showed that both magnitude and phase are relatively flat through excited frequencies up to $100\,\mathrm{Hz}$, indicating that the sensor is suitable for both static and dynamic sensing applications.

Figure 4 shows net force on the leg measured by the tactile sensors compared to data from the ATI force/torque sensor mounted beneath various materials on a test platform (Fig. 5) for a single stride. The data are comparable, with minor differences due to leg bending and the distribution of the ground reaction force over multiple taxels.

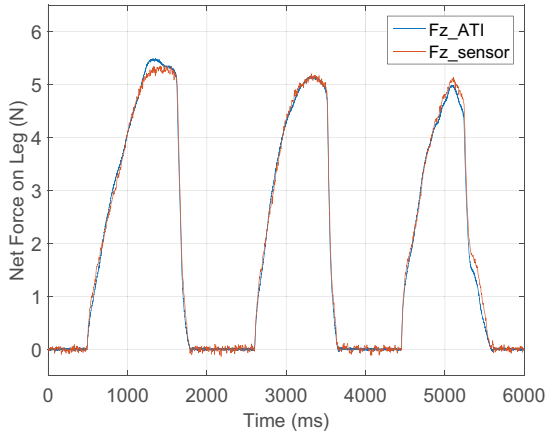

Fig. 3: Calibrated sensor performance compared to ATI load cell for an arbitrary force trajectory (static uniaxial compression).

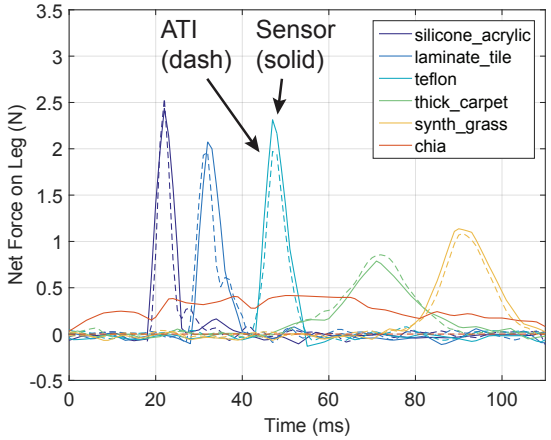

Fig. 4: Calibrated single stride sensor data (solid) compared to ATI load cell GRF data (dashed) over different terrains at 10 Hz leg frequency. Due to practical difficulties, it was not possible to collect ATI data for running on granular media (chia seeds).

IV. Robot Performance and Terrain Selection

A. Bipedal Runner

A two-legged runner (Fig. 1, Fig. 5), conceptually similar to previous tethered runners that run in a circle [52]–[54], albeit at a much smaller scale, was built to measure running performance and ground reaction forces on a range of test surfaces. The mass and dimensions are chosen to approximate the behavior of small legged robots such as EduBot/SandBot [1], Mini-Whegs [55] and the RoACH class of robots [4,5], which employ curved legs for locomotion.

Two C-shaped legs are attached to the motor shaft (Maxon DCX10L EB KL 12V, 16:1 planetary gearhead), 180 degrees apart. The motor and legs are mounted on a 3D printed two-axis gimbal structure that allows the entire assembly to pivot freely about the vertical and horizontal axes. Adjusting the counterbalancing allows one to control the effective inertia and gravity force on the legs. Depending on balance, speed and terrain type, the legs can walk, with little vertical motion, or trot, with a significant hopping height on a circular track with interchangeable terrain surfaces. Specifications of the apparatus are provided in Table I.

Slip-rings connect wires from the rotating frames to a fixed frame. A through bore slip-ring (Orbex Group, 503-0600) connects wires from rotating leg sensors to the computer. Another double slip-ring setup (Adafruit) connects all the wires from the pivoting motor mount to a fixed frame. An encoder (AVAGO HEDM 5500) measures the horizontal pivot angle and robot body velocity. The same ATI sensor as used for sensor calibration is installed beneath a portion of the circular track to measure GRF for comparison to leg sensor signals. A microprocessor (Texas Instruments TM4C123GH6PM) is used for closed-loop stride frequency control and quadrature encoder measurements at 1 kHz.

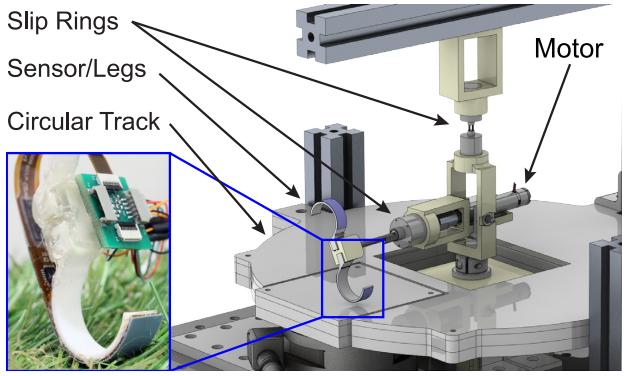

Fig. 5: Two-legged runner and gimbal apparatus with instrumented curved legs and circular track with interchangeable surfaces.

TABLE I: Specifications for two-legged running robot.

Parameter (μ)	Value	Units
Effective mass (vertical contacts)	7.8	g
Effective mass (horizontal)	5.7	g
Leg mass	0.43	g
Leg length	30	mm
Leg stiffness	1325	N/m
Motor stall torque	4.38	mNm
Motor no load speed	11200	rpm
Gear ratio	16:1	
Pivot radius	105	mm

B. Terrain Selection

Six representative terrain types, with variations in friction and hardness, were prepared for GRF sensing and classification experiments (Fig. 6 and Table II).

V. Methods

A. Running Experiments

For each selected surface, stride frequencies from 6-16 Hz by 2 Hz increments were examined. This frequency range was chosen because it covers walking and running behavior of the apparatus. For each terrain, 72 seconds of running data were

Fig. 6: Surfaces used in experiment (described in Table II).

TABLE II: Terrains used in GRF sensing experiments; machine learning class labels listed in Section V-C.

Terrain	Description	Friction Coefficient (μ)	Penetration Depth (mm)	Class Label
1	125 µm shore10A silicone-lined acrylic	1.6	0	HF
2	laminate tile	1.3	0	HF
3	Teflon	0.04	0	LF
4	thick-pile carpet	0.9	7	D
5	synthetic grass	1.1	4	D
6	chia seeds	0.6	12	G

collected for each stride frequency. For all ground surfaces except PTFE (Teflon) sheet, the silicone outer skin of the leg made contact directly with the surface; for Teflon, the leg was wrapped in a thin film of PTFE tape because silicone/Teflon contact has high adhesion and does not slip at light loads. High speed videos were recorded at 400 fps to observe ground interactions in detail. However, these visual data were not used for terrain classification.[1]

Figure 7 shows the behavior of the robot on different surfaces at each stride frequency. For all surfaces, the apparatus is predominantly walking at 6 Hz. On surfaces 1, 2, 4, and 5, the robot demonstrated the most consistent running behavior and the lowest variations in forward body velocity at 10 Hz. Beyond 10 Hz the robot began to exhibit some airborne behavior. This hopping behavior is most noticeable at frequencies above 14 Hz on thick carpet and synthetic grass. On Teflon, the apparatus stalled due to slip at 8 Hz and 14 Hz, but managed to propel itself forward sporadically at other frequencies. In the granular chia seeds, the runner consistently increased its forward body speed with increasing stride frequency, indicating that this terrain had a qualitatively viscous effect on locomotion.

B. Feature Extraction

In order to examine GRF when the leg is in contact with the ground, we segmented the data into strides based on the contact period associated with each stride frequency. A peak detection algorithm was used to find the peak sensor force (calculated as the maximum absolute value of summation of 5 taxel signals) within the stride period. After the peaks were found, the start and end points of each stride were determined via thresholding with respect to the RMS value of the sensor noise floor. In the end, 150 ground contact stride segments from every frequency were extracted for each of the terrains tested.

[1]Videos can be found in the multimedia extension and at: http://bdml.stanford.edu/Main/BipedalRunnerExperiments

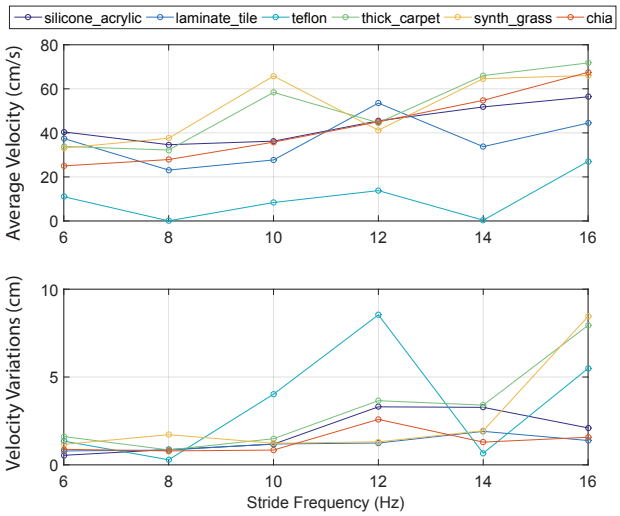

Fig. 7: Average body velocity and velocity RMSE across different surfaces.

We are interested in performing terrain identification using data obtained from each robot stride. Accordingly, relevant sensor and motor torque waveform features that captured the characteristics of leg/ground interactions were extracted from each stride segment for training and testing our classifier. In addition to sensor and motor information, stride frequency is used as a classifier feature since the walking or running dynamics of the apparatus vary with stride frequency. A similar strategy was adopted by [29,56] to allow terrain classifiers to adapt to different dynamic regimes. Table III lists features used by the classifier.

TABLE III: Machine Learning Feature Set

Index	Feature Name
1	Robot stride frequency
2	Sensor force (net) peak amplitude
3	Sensor force (net) width
4	Sensor force (net) area under curve (impulse)
5	Motor torque peak amplitude
6	Peak motor torque:peak sensor force ratio
7	Sensor force (net) average amplitude
8	Motor torque average amplitude
9	Average motor torque:average sensor force ratio
10	Motor torque width
11	Motor torque area under curve
12-16	Individual taxel (1-5) force peak amplitude

C. Machine Learning

We posit that a terrain classifier for gait adaptation is useful when it can inform a robot of the locomotion-related properties of the surface it is walking on. Such a terrain classifier is most helpful when the robot is transitioning between two disparate surfaces (such as running on a surface like concrete versus running on a softer and more dissipative surface like sand) rather than two similar surfaces (such as transitioning from

concrete to a plastic laminate floor). From Figs. 4 and 7, we see that the ground reaction forces and average body velocity are similar for surfaces with comparable friction and stiffness. Prior work by [18] similarly suggests that terrain classification based on physical properties will better reflect the influence of the terrain type on the robotic gait and lead to improved terrain classification results.

To train and test our classifier, we combined sensor and motor torque data from the 6 terrains into 4 representative terrain classes based on their friction and stiffness properties: 1) a high friction hard surface class (HF) consisting of the thin silicone-lined acrylic surface and the laminate tile; 2) a low friction hard surface class (LF) consisting of Teflon; 3) a deformable surface class (D) consisting of thick-pile carpet and synthetic grass; and 4) a granular class (G) consisting of chia seeds. Since the LF and G classes only contain data from one type of terrain, we randomly sampled an equal amount of data from the HF and G classes to form an overall data set consisting of 3600 total instances (stride segments), with 900 instances from each class.

We used WEKA 3.7 [57] for classifier training and testing. Our classifier is a support vector machine (SVM) trained via a sequential minimal optimization (SMO) algorithm using the Pearson VII function-based universal kernel (PUK) [58,59]. Classifier accuracy is evaluated using 10-fold cross-validation. We used an SMO-based SVM classifier because of its versatility, speed and robustness. SVM classifiers have also demonstrated good results when used for terrain classification based on high-frequency vibration signals [8,29,60].

Since the characteristics and distribution of our feature set have not been well studied previously, it is difficult to optimize kernel selection for our classifier without time-consuming optimization procedures. Compared to linear, polynomial and RBF kernel functions, the PUK has been shown to be a robust and generic alternative capable of providing equal or better mapping than traditional SVM kernels, leading to an equal or better generalization performance of SVMs [59]. Note that WEKA's SMO implementation solves multi-class problems via pairwise classification [61].

VI. Results and Discussion

A. Ground Reaction Force Sensing

Figure 8 shows normal GRF data for each of the 5 taxels on four different surfaces. Qualitatively we see that on a stiff surface, most of the force is concentrated on a single taxel over a short period of time. On a deformable surface such as thick carpet, the force profile becomes more temporally distributed and covers multiple neighboring taxels. Lastly, we see that in granular material, through the first phase of the stride (0-50ms), the proximal taxel 5 experiences most of the ground contact force as the leg penetrates down and backwards into the granular material. This first push displaces some of the material and propels the body forward. Due to the curved shaped of the leg, neighboring taxels 2-4 experience mostly shear forces (not captured by the normal force taxels) as the leg begins to slip tangentially in the circular depression surrounding the first impact. In the second phase of the stride (50-120ms) the distal tip of the leg (taxel 1) starts to make contact with the surface and experiences normal force loads as the leg further displaces the granular material.

Visualization of three classification features (peak amplitude, width, area under curve) at a constant stride frequency demonstrates qualitatively the separation of terrain classes into distinct populations (Fig. 9).

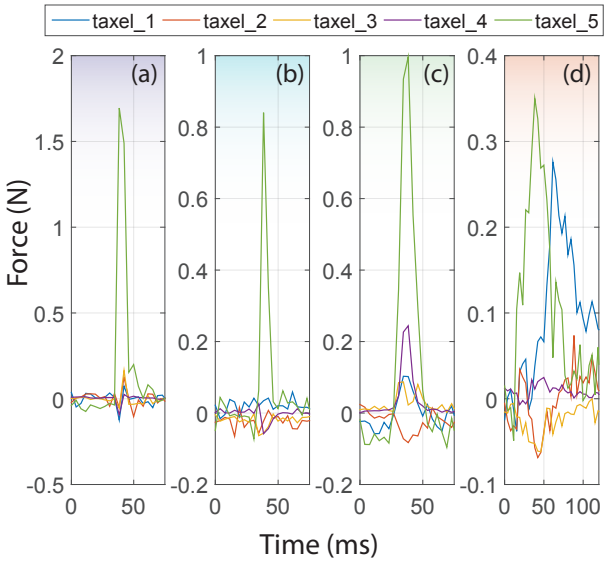

Fig. 8: Individual taxel forces recorded on different surfaces at 10 Hz stride frequency, from left: a) silicone-lined acrylic, b) teflon, c) thick-carpet, d) chia seeds.

B. Terrain Classifier Performance

Using the full feature set (Table III), the classifier achieves an overall accuracy of 94.4% for terrain classification across the 4 terrain classes (HF, LF, D, G). Table IV shows that the classifier performed best on granular surfaces, with an accuracy of 98.4% and worst on low-friction surfaces, with an accuracy of 92.7%. In general, stiff, high friction surfaces are more likely to be misclassified as low-friction surfaces, and vice versa, since both surfaces have low deformability, so peak and average sensor readings can be similar.

In addition to high accuracy and robustness, the terrain classifier demonstrates the potential for real-time implementation with offline model parameter fitting. Using the MATLAB profiler (1000 executions, 1 ms clock precision, 2.6 GHz clock speed) under Windows 7 OS without code optimization, our classifier trains the SVM in 2 seconds while executing terrain classifications in 1 ms per stride on average.

C. Sensor Feature Analysis

We performed feature analysis on our classifier using a greedy stepwise search algorithm to develop insights into the best sensor features for terrain classification. Feature merit scores are presented in Fig. 10. Results show that the top three features with the best scores are motor torque amplitude, frequency, and torque area under curve.

In the present case, with a single motor directly connected to the shaft propelling the legs, the motor torque is a good

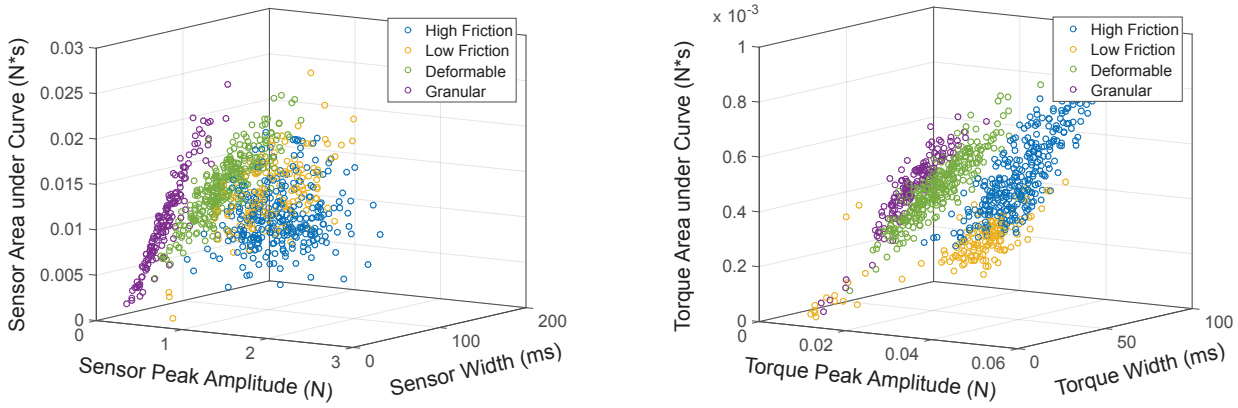

(a) Tactile sensor feature space

(b) Motor torque feature space

Fig. 9: Selective plot of classifier features at 10 Hz stride frequency: tactile sensor (right) and motor torque (left).

TABLE IV: Terrain classifier performance using complete feature set from Table III.

		Predicted Class			
		High friction (Hf)	Low friction (Lf)	Deformable (D)	Granular (G)
True Class	High friction (Hf)	92.89%	4.44%	2.56%	0.11%
	Low friction (Lf)	5.89%	92.67%	1.00%	0.44%
	Deformable (D)	1.22%	3.67%	93.44%	1.67%
	Granular (G)	0.00%	0.78%	0.78%	98.44%

TABLE V: Terrain classifier performance using only stride frequency and tactile sensor features.

		Predicted Class			
		High friction (Hf)	Low friction (Lf)	Deformable (D)	Granular (G)
True Class	High friction (Hf)	84.33%	13.00%	2.56%	0.11%
	Low friction (Lf)	5.89%	84.11%	6.67%	3.33%
	Deformable (D)	1.33%	9.89%	86.00%	2.78%
	Granular (G)	0.00%	0.78%	0.44%	98.78%

TABLE VI: Terrain classifier performance using only stride frequency and motor torque features.

		Predicted Class			
		High friction (Hf)	Low friction (Lf)	Deformable (D)	Granular (G)
True Class	High friction (Hf)	84.56%	9.44%	5.33%	0.67%
	Low friction (Lf)	13.33%	80.22%	0.67%	5.78%
	Deformable (D)	3.22%	3.00%	84.33%	9.44%
	Granular (G)	0.00%	5.56%	1.44%	93.00%

indication of the effort required to move at a particular speed. It is also closely related to the horizontal ground reaction force. Hence it is not surprising that the motor peak and average torque are especially useful features for terrain classification. However, in other small robots the connection between the motor and the legs maybe less direct and a single motor may be driving all the legs – those in stance and those in flight. In such cases the peak motor torque may be a less useful feature. Therefore, to evaluate the effectiveness of sensor features and stride frequency alone, we re-trained and tested the classifier with a subset of features.

Using only sensor data and stride frequency as training features, we achieved 88.3% overall accuracy (worst accuracy for low-friction of 84.1% and best for granular media of 98.8%). When motor torque information is not present, sensor peak force and area under the curve had the highest influence on classifier accuracy (Fig. 10). Using only motor torque and stride frequency as training features, we achieved 85.5% overall accuracy (again, worst for low-friction, LF, and best for granular media, G). Thus, where peak motor torque is not a reliable indication of the peak ground reaction force, using the tactile sensors alone can produce a relatively reliable terrain classification.

Note also that we are currently performing terrain classification with data from a single stride. In practice, the accuracy should improve if results from multiple consecutive steps are considered since terrain data maybe spatially and temporally correlated [62].

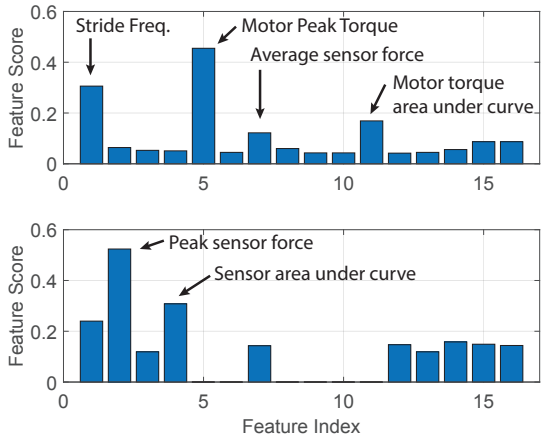

Fig. 10: Feature scores across all training features (top), feature scores across only sensor features and stride frequency (bottom); higher scores indicate more contribution to classifier accuracy. Feature index provided in Table III.

VII. Conclusions and Future Work

A. Conclusions

We present the design and use of an array of capacitive tactile sensors mounted on a flexible printed circuit with local

signal processing and communications, intended to measure the ground reaction forces for small legged robots.

Using signal features from the sensors, we were able to train and test a SVM classifier to perform single stride terrain classification with better than 90% accuracy on several representative types of terrain. For the apparatus tested, the peak and average motor torque were directly related to the ground reaction forces and yielded the highest classifier feature scores. When this information is not available, or is not as well correlated with ground forces, using only the tactile sensor data and information about stride frequency can also provide a reliable terrain identification in most cases.

B. Future Work

1) Sensor Development: For an arbitrary terrain, a robot's leg motor torque information is related to kinetic friction and to the effort required to maintain velocity on dissipative terrain. The normal force taxels provide information related to surface deformability. A full-package sensing solution would measure both normal force and either shear force along the leg or torque where the leg is attached to its shaft. The availability of this information at rates above 100 Hz makes closed-loop gait control and adaptation possible.

2) Applications: In this work we attached our tactile sensors to a C-shaped leg. However, the tactile sensor can easily be adapted to other leg shapes and sizes. For example, the sensor can easily be scaled for heavier loads in larger robots simply by adjusting the stiffness of the dielectric layer. In the near future we hope to attach the sensor to a small quadrupedal or hexapedal robot to capture live GRF measurements and perform real-time terrain classification. We would also like to perform terrain identification on a greater variety of outdoor surfaces such as soil, gravel and sand, to study the robustness of our classifier on these complex deformable terrains. Furthermore, we hope to use the sensors to characterize robot leg collisions with obstacles, which could permit more robust trajectory control in cluttered terrain [63].

REFERENCES

[1] C. Li, P. B. Umbanhowar, H. Komsuoglu, D. E. Koditschek, and D. I. Goldman, "Sensitive dependence of the motion of a legged robot on granular media," *Proceedings of the National Academy of Sciences*, vol. 106, no. 9, pp. 3029–3034, 2009.

[2] F. Qian and D. I. Goldman, "The dynamics of legged locomotion in heterogeneous terrain: universality in scattering and sensitivity to initial conditions," in *Robotics: Science and Systems*.

[3] F. Delcomyn, M. E. Nelson, and J. H. Cocatre-Zilgien, "Sense organs of insect legs and the selection of sensors for agile walking robots," *IJRR*, vol. 15, no. 2, pp. 113–127, 1996.

[4] D. W. Haldane, K. C. Peterson, F. L. Garcia Bermudez, and R. S. Fearing, "Animal-inspired design and aerodynamic stabilization of a hexapedal millirobot," in *ICRA*, pp. 3279–3286, IEEE, 2013.

[5] A. O. Pullin, N. J. Kohut, D. Zarrouk, and R. S. Fearing, "Dynamic turning of 13 cm robot comparing tail and differential drive," in *ICRA*, pp. 5086–5093, IEEE, 2012.

[6] L. Ojeda, J. Borenstein, G. Witus, and R. Karlsen, "Terrain characterization and classification with a mobile robot," *Journal of Field Robotics*, vol. 23, no. 2, pp. 103–122, 2006.

[7] C. Brooks, K. Iagnemma, *et al.*, "Vibration-based terrain classification for planetary exploration rovers," *IEEE Trans. on Robotics*, vol. 21, no. 6, pp. 1185–1191, 2005.

[8] C. Weiss, H. Frohlich, and A. Zell, "Vibration-based terrain classification using support vector machines," in *IEEE/RSJ IROS*, pp. 4429–4434, IEEE, 2006.

[9] C. A. Brooks and K. Iagnemma, "Self-supervised terrain classification for planetary surface exploration rovers," *Journal of Field Robotics*, vol. 29, no. 3, pp. 445–468, 2012.

[10] C. Ordonez, J. Shill, A. Johnson, J. Clark, and E. Collins, "Terrain identification for rhex-type robots," in *SPIE Defense, Security, and Sensing*, pp. 87410Q–87410Q, International Society for Optics and Photonics, 2013.

[11] A. Angelova, L. Matthies, D. Helmick, and P. Perona, "Fast terrain classification using variable-length representation for autonomous navigation," in *Computer Vision and Pattern Recognition, 2007. CVPR'07. IEEE Conference on*, pp. 1–8, IEEE, 2007.

[12] P. Filitchkin and K. Byl, "Feature-based terrain classification for littledog," in *IEEE/RSJ IROS*, pp. 1387–1392, IEEE, 2012.

[13] K. Walas and M. Nowicki, "Terrain classification using laser range finder," in *IEEE/RSJ IROS*, pp. 5003–5009, IEEE, 2014.

[14] S. Zenker, E. E. Aksoy, D. Goldschmidt, F. Worgotter, and P. Manoonpong, "Visual terrain classification for selecting energy efficient gaits of a hexapod robot," in *Advanced Intelligent Mechatronics (AIM), 2013 IEEE/ASME International Conference on*, pp. 577–584, IEEE, 2013.

[15] D. W. Haldane, P. Fankhauser, R. Siegwart, and R. S. Fearing, "Detection of slippery terrain with a heterogeneous team of legged robots," in *ICRA*, pp. 4576–4581, IEEE, 2014.

[16] J. Libby and A. J. Stentz, "Using sound to classify vehicle-terrain interactions in outdoor environments," in *Robotics and Automation (ICRA), 2012 IEEE International Conference on*, pp. 3559–3566, IEEE, 2012.

[17] P. Giguere and G. Dudek, "A simple tactile probe for surface identification by mobile robots," *IEEE Trans. on Robotics*, vol. 27, no. 3, pp. 534–544, 2011.

[18] K. Walas, "Terrain classification using vision, depth and tactile perception," *Proceedings of the 2013 RGB-D: Advanced Reasoning with Depth Cameras in Conjunction with RSS, Berlin, Germany*, vol. 27, 2013.

[19] A. Schmidt and K. Walas, "The classification of the terrain by a hexapod robot," in *Proceedings of the 8th International Conference on Computer Recognition Systems CORES 2013*, pp. 825–833, Springer, 2013.

[20] M. Höpflinger, C. D. Remy, M. Hutter, L. Spinello, R. Siegwart, *et al.*, "Haptic terrain classification for legged robots," in *ICRA*, pp. 2828–2833, IEEE, 2010.

[21] L. Ascari, M. Ziegenmeyer, P. Corradi, B. Gaßmann, M. Zöllner, R. Dillmann, and P. Dario, "Can statistics help walking robots in assessing terrain roughness? platform description and preliminary considerations," in *Prooceedings of the 9th ESA Workshop on Advanced Space Technologies for Robotics and Automation ASTRA2006, ESTEC, Noordwijk, The Netherlands*, 2006.

[22] S. C. Peters and K. Iagnemma, "An analysis of rollover stability measurement for high-speed mobile robots," in *Robotics and Automation, 2006. ICRA 2006. Proceedings 2006 IEEE International Conference on*, pp. 3711–3716, IEEE, 2006.

[23] D. Odenthal, T. Bunte, and J. Ackermann, "Nonlinear steering and braking control for vehicle rollover avoidance," in *Proceedings of European Control Conference*, Karlsruhe Germany, 1999.

[24] C. Klein, S. Kittivatcharapong, *et al.*, "Optimal force distribution for the legs of a walking machine with friction cone constraints," *Robotics and Automation, IEEE Transactions on*, vol. 6, no. 1, pp. 73–85, 1990.

[25] L. Righetti, J. Buchli, M. Mistry, M. Kalakrishnan, and S. Schaal, "Optimal distribution of contact forces with inverse-dynamics control," *The International Journal of Robotics Research*, vol. 32, no. 3, pp. 280–298, 2013.

[26] S. S. Roy and D. K. Pratihar, "Effects of turning gait parameters on energy consumption and stability of a six-legged walking robot," *Robotics and Autonomous Systems*, vol. 60, no. 1, pp. 72–82, 2012.

[27] D. W. Haldane, C. S. Casarez, J. T. Karras, J. Lee, C. Li, A. O. Pullin, E. W. Schaler, D. Yun, H. Ota, A. Javey, *et al.*, "Integrated manufacture of exoskeletons and sensing structures for folded millirobots," *Journal of Mechanisms and Robotics*, vol. 7, no. 2, p. 021011, 2015.

[28] S. S. Desai, A. M. Eckert-Erdheim, and A. M. Hoover, "A large-area tactile force sensor for measuring ground reaction forces from small legged robots," in *IEEE/RSJ IROS*, pp. 4753–4758, IEEE, 2013.

[29] F. L. Garcia Bermudez, R. C. Julian, D. W. Haldane, P. Abbeel, and R. S. Fearing, "Performance analysis and terrain classification for a legged robot over rough terrain," in *IEEE/RSJ IROS*, pp. 513–519, IEEE, 2012.

[30] M. R. Cutkosky and J. Ulmen, "Dynamic tactile sensing," in *The Human Hand as an Inspiration for Robot Hand Development*, pp. 389–403, Springer, 2014.

[31] R. S. Dahiya, G. Metta, M. Valle, and G. Sandini, "Tactile sensing—from humans to humanoids," *Robotics, IEEE Transactions on*, vol. 26, no. 1, pp. 1–20, 2010.

[32] H. Yousef, M. Boukallel, and K. Althoefer, "Tactile sensing for dexterous in-hand manipulation in robotics—a review," *Sensors and Actuators A: physical*, vol. 167, no. 2, pp. 171–187, 2011.

[33] M. R. Cutkosky, R. D. Howe, and W. R. Provancher, "Force and tactile sensors," in *Springer Handbook of Robotics*, pp. 455–476, Springer, 2008.

[34] M. Quigley, C. Salisbury, A. Y. Ng, and J. K. Salisbury, "Mechatronic design of an integrated robotic hand," *The International Journal of Robotics Research*, vol. 33, no. 5, pp. 706–720, 2014.

[35] B. Ali, M. A. Ayub, and H. Yussof, "Characteristics of a new optical tactile sensor for interactive robot fingers," *International Journal of Social Robotics*, vol. 4, no. 1, pp. 85–91, 2012.

[36] Y. Ohmura, Y. Kuniyoshi, and A. Nagakubo, "Conformable and scalable tactile sensor skin for curved surfaces," in *Robotics and Automation, 2006. ICRA 2006. Proceedings 2006 IEEE International Conference on*, pp. 1348–1353, IEEE, 2006.

[37] Y. Yamada, T. Morizono, Y. Umetani, and H. Takahashi, "Highly soft viscoelastic robot skin with a contact object-location-sensing capability," *Industrial Electronics, IEEE Transactions on*, vol. 52, no. 4, pp. 960–968, 2005.

[38] Y.-L. Park, B.-R. Chen, and R. J. Wood, "Design and fabrication of soft artificial skin using embedded microchannels and liquid conductors," *Sensors Journal, IEEE*, vol. 12, no. 8, pp. 2711–2718, 2012.

[39] K. Takei, Z. Yu, M. Zheng, H. Ota, T. Takahashi, and A. Javey, "Highly sensitive electronic whiskers based on patterned carbon nanotube and silver nanoparticle composite films," *Proceedings of the National Academy of Sciences*, vol. 111, no. 5, pp. 1703–1707, 2014.

[40] S. Harada, K. Kanao, Y. Yamamoto, T. Arie, S. Akita, and K. Takei, "Fully printed flexible fingerprint-like three-axis tactile and slip force and temperature sensors for artificial skin," *ACS nano*, vol. 8, no. 12, pp. 12851–12857, 2014.

[41] J. B. Gafford, S. B. Kesner, A. Degirmenci, R. J. Wood, R. D. Howe, and C. J. Walsh, "A monolithic approach to fabricating low-cost, millimeter-scale multi-axis force sensors for minimally-invasive surgery," in *Robotics and Automation (ICRA), 2014 IEEE International Conference on*, pp. 1419–1425, IEEE, 2014.

[42] S. Takenawa, "A magnetic type tactile sensor using a two-dimensional array of inductors," in *Robotics and Automation, 2009. ICRA'09. IEEE International Conference on*, pp. 3295–3300, IEEE, 2009.

[43] J.-i. Yuji and S. Shiraki, "Magnetic tactile sensing method with hall element for artificial finger," in *Sensing Technology (ICST), 2013 Seventh International Conference on*, pp. 311–315, IEEE, 2013.

[44] A. Shashank, M. Tiwana, S. Redmond, and N. Lovell, "Design, simulation and fabrication of a low cost capacitive tactile shear sensor for a robotic hand," in *IEEE EMBC*, pp. 4132–4135, IEEE, 2009.

[45] J. Ulmen and M. Cutkosky, "A robust, low-cost and low-noise artificial skin for human-friendly robots," in *IEEE ICRA*, pp. 4836–41, 2010.

[46] A. Schmitz, P. Maiolino, M. Maggiali, L. Natale, G. Cannata, and G. Metta, "Methods and technologies for the implementation of large-scale robot tactile sensors," *Robotics, IEEE Transactions on*, vol. 27, no. 3, pp. 389–400, 2011.

[47] D. M. Aukes, B. Heyneman, J. Ulmen, H. Stuart, M. R. Cutkosky, S. Kim, P. Garcia, and A. Edsinger, "Design and testing of a selectively compliant underactuated hand," *IJRR*, p. 0278364913518997, 2014.

[48] M. Maggiali, G. Cannata, P. Maiolino, G. Metta, M. Randazzo, and G. Sandini, "Embedded distributed capacitive tactile sensor," in *Mechatronics Forum Biennial International Conference 2008, University of Limerick, Ireland,*, June 2008.

[49] B. Heyneman and M. R. Cutkosky, "Slip classification for dynamic tactile array sensors," *IJRR*, p. 0278364914564703, 2015.

[50] U. Kim, D.-H. Lee, H. Moon, J. C. Koo, and H. R. Choi, "Design and realization of grasper-integrated force sensor for minimally invasive robotic surgery," in *IEEE/RSJ IROS*, pp. 4321–4326, IEEE, 2014.

[51] B. Heyneman and M. R. Cutkosky, "Biologically inspired tactile classification of object-hand and object-world interactions," in *Robotics and Biomimetics (ROBIO), 2012 IEEE International Conference on*, pp. 167–173, IEEE, 2012.

[52] D. Koepl and J. Hurst, "Impulse control for planar spring-mass running," *Journal of Intelligent & Robotic Systems*, vol. 74, no. 3-4, pp. 589–603, 2014.

[53] J. Grizzle, J. Hurst, B. Morris, H.-W. Park, and K. Sreenath, "Mabel, a new robotic bipedal walker and runner," in *American Control Conference, 2009. ACC'09.*, pp. 2030–2036, IEEE, 2009.

[54] J. K. Hodgins and M. H. Raibert, "Adjusting step length for rough terrain locomotion," *Robotics and Automation, IEEE Trans. on*, vol. 7, no. 3, pp. 289–298, 1991.

[55] J. M. Morrey, B. Lambrecht, A. D. Horchler, R. E. Ritzmann, and R. D. Quinn, "Highly mobile and robust small quadruped robots," in *IEEE/RSJ IROS*, vol. 1, pp. 82–87, IEEE, 2003.

[56] E. Coyle and E. G. Collins Jr, "A comparison of classifier performance for vibration-based terrain classification," tech. rep., DTIC Document, 2008.

[57] M. Hall, E. Frank, G. Holmes, B. Pfahringer, P. Reutemann, and I. H. Witten, "The weka data mining software: an update," *ACM SIGKDD explorations newsletter*, vol. 11, no. 1, pp. 10–18, 2009.

[58] J. Platt *et al.*, "Fast training of support vector machines using sequential minimal optimization," *Advances in kernel methods—support vector learning*, vol. 3, 1999.

[59] B. Üstün, W. J. Melssen, and L. M. Buydens, "Facilitating the application of support vector regression by using a universal pearson vii function based kernel," *Chemometrics and Intelligent Laboratory Systems*, vol. 81, no. 1, pp. 29–40, 2006.

[60] C. Weiss, N. Fechner, M. Stark, and A. Zell, "Comparison of different approaches to vibration-based terrain classification.," in *EMCR*, 2007.

[61] T. Hastie, R. Tibshirani, *et al.*, "Classification by pairwise coupling," *The annals of statistics*, vol. 26, no. 2, pp. 451–471, 1998.

[62] P. Giguere and G. Dudek, "Clustering sensor data for autonomous terrain identification using time-dependency," *Autonomous Robots*, vol. 26, no. 2-3, pp. 171–186, 2009.

[63] F. Qian and D. Goldman, "Anticipatory control using substrate manipulation enables trajectory control of legged locomotion on heterogeneous granular media," in *SPIE Defense+ Security*, International Society for Optics and Photonics, 2015.